International Conference on Textile Composites and Inflatable Structures
STRUCTURAL MEMBRANES 2011
E. Oñate, B. Kröplin and K.-U.Bletzinger (Eds)

SPACE–TIME FSI MODELING OF RINGSAIL PARACHUTE CLUSTERS

KENJI TAKIZAWA*, TIMOTHY SPIELMAN† AND TAYFUN E. TEZDUYAR†

*Department of Modern Mechanical Engineering and
Waseda Institute for Advanced Study, Waseda University
1-6-1 Nishi-Waseda, Shinjuku-ku, Tokyo 169-8050, JAPAN

†Mechanical Engineering, Rice University – MS 321
6100 Main Street, Houston, TX 77005, USA

Key words: Fluid–structure interaction, Parachute clusters, Ringsail parachute, Space–time technique, Geometric porosity, Contact

Abstract. The computational challenges posed by fluid–structure interaction (FSI) modeling of ringsail parachute clusters include the lightness of the membrane and cable structure of the canopy compared to the air masses involved in the parachute dynamics, geometric complexities created by the construction of the canopy from "rings" and "sails" with hundreds of ring gaps and sail slits, and the contact between the parachutes. The Team for Advanced Flow Simulation and Modeling (T★AFSM) has successfully addressed these computational challenges with the Stabilized Space–Time FSI technique (SSTFSI), which was developed and improved over the years by the T★AFSM and serves as the core numerical technology, and a number of special techniques developed in conjunction with the SSTFSI. We present the results obtained with the FSI computation of parachute clusters and the related dynamical analysis.

1 INTRODUCTION

Fluid–structure interaction (FSI) modeling of ringsail parachute clusters poses a number of computational challenges. The membrane and cable structure of the canopy is much lighter compared to the air masses involved in the parachute dynamics, and this requires a robust FSI coupling technique. This challenge is of course not limited to ringsail parachutes but is common to all parachute FSI computations. The geometric challenge created by the construction of the canopy from "rings" and "sails" with hundreds of ring gaps and sail slits requires a computational model that makes the problem tractable. Contact between the parachutes requires an algorithm that protects the fluid mechanics

mesh from excessive deformation, and this computational challenge might also be encountered in other classes of FSI problems where two solid surfaces come into contact. The Team for Advanced Flow Simulation and Modeling (T★AFSM) has successfully addressed these computational challenges with the Stabilized Space–Time FSI technique (SSTFSI), which was developed and improved over the years by the T★AFSM and serves as the core numerical technology, and special techniques developed in conjunction with the SSTFSI.

The SSTFSI technique was introduced in [1]. It is based on the new-generation Deforming-Spatial-Domain/Stabilized Space–Time (DSD/SST) formulations, which were also introduced in [1], increasing the scope and performance of the DSD/SST formulations developed earlier [2, 3, 4, 5] for computation of flows with moving boundaries and interfaces, including FSI. This core technology was used in a large number of parachute FSI computations (see, for example, [1, 6, 7, 8, 9, 10, 11, 12]). The direct and quasi-direct FSI coupling techniques, which are generalizations of the monolithic solution techniques to cases with incompatible fluid and structure meshes at the interface, were introduced in [13]. They provide robustness even in computations where the structure is light compared to the fluid masses involved in the dynamics of the FSI problem and were also used in a large number of parachute FSI computations (see, for example, [1, 6, 7, 8, 9, 10, 11, 12]). Computer modeling of large ringsail parachutes by the T★AFSM was first reported in [6, 7]. The geometric challenge created by the ringsail construction was addressed with the Homogenized Modeling of Geometric Porosity (HMGP) [6], adaptive HMGP [8] and a new version of the HMGP that is called "HMGP-FG" [9]. Additional special techniques the T★AFSM introduced in the context of ringsail parachutes include the FSI Geometric Smoothing Technique (FSI-GST) [1], Separated Stress Projection (SSP) [6], "symmetric FSI" technique [8], a method that accounts for the fluid forces acting on structural components (such as parachute suspension lines) that are not expected to influence the flow [8], and other interface projection techniques [14].

The T★AFSM recently started addressing (see [10, 11]) the challenge created by the contact between the parachutes. In a contact algorithm to be used in this context, the objective is to prevent the structural surfaces from coming closer than a predetermined minimum distance we would like to maintain to protect the quality of the fluid mechanics mesh between the structural surfaces. The Surface-Edge-Node Contact Tracking (SENCT) technique was introduced in [1] for this purpose. It had two versions: SENCT-Force (SENCT-F) and SENCT-Displacement (SENCT-D). In the SENCT-F technique, which is the relevant version here, the contacted node is subjected to penalty forces that are inversely proportional to the projection distances to the contacting surfaces, edges and nodes. For FSI problems with incompatible fluid and structure meshes at the interface, it was proposed in Remark 1 of [6] to formulate the contact model based on the fluid mechanics mesh at the interface. This version of the SENCT was denoted with the option key "-M1". The contact algorithm used in the parachute cluster computations reported in [10] has some features in common with the SENCT-F technique but is more robust. Also, compared to the SENCT-F technique, the forces are applied in a conserva-

tive fashion. We call the new technique "SENCT-FC", where the letter "C" stands for "conservative". The new technique was used with option M1 in [10]. The SENCT-FC technique was described in detail in [11] and was used with option M1 also in the cluster computations reported in that article. This short article uses material from [11]. We present the computational results together with the related dynamical analysis.

2 CLUSTER COMPUTATIONS

A series of two-parachute cluster computations were carried out in [11] to determine how the parameters representing the payload models and starting conditions affect long-term cluster dynamics. The parachute clusters reported in [11] were used with a 19,200 lb payload. Each parachute has 80 gores and 4 rings and 9 sails, with 4 ring gaps and 8 sail slits. Figure 1 shows, for an inflated ringsail parachute from [9], the ring and sail construction and the ring gaps and sail slits. More information on the parachutes can be

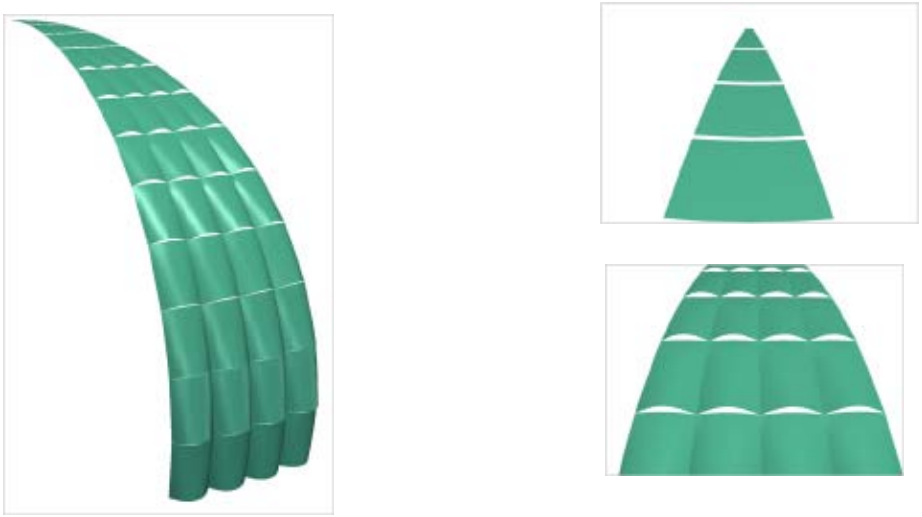

Figure 1: A four-gore slice of a ringsail parachute in its inflated form. The pictures on the right illustrate the ring and sail construction of the canopy and show the shapes of the ring gaps and sail slits.

found in [7, 8, 9]. The parameters selected for testing were the payload-model configurations and initial coning angles (θ_{INIT}) and parachute diameters (D_{INIT}) (for readers not familiar with the term "coning angle", see [11]). We also investigated two scenarios to approximate the conditions immediately after parachute disreefing. This is explained in more detail in a later paragraph. In all cases, the θ_{INIT} is the same for both parachutes

The first set of computations were carried out to investigate the effect of the payload model. In drop tests, the parachutes are connected to a rectangular pallet that is weighted to represent the mass and inertial properties of a proposed crew capsule. The preliminary parachute cluster computations reported in [10] modeled the payload as a point mass located at the confluence of the risers. We will refer to this as the payload at the confluence

(PAC) configuration. Two new computational payload models were created to see how they would influence parachute behavior. The payload lower than the confluence (PLC) configuration adds another cable element below the confluence and models the payload as a point mass at the location of the pallet center of gravity. The payload as a truss element (PTE) configuration further enhances the model by distributing the payload mass at 9 different points to match the mass, center of gravity, and six components of the inertia tensor of the pallet. This is accomplished by adding 5 cable elements and 26 truss elements below the confluence. In all of the payload comparison computations, $\theta_{\text{INIT}} = 35^\circ$.

The second set of computations were carried out to investigate the effect of θ_{INIT}. Three values of θ_{INIT} were tested: 15°, 25°, and 35°. It should be noted that 35° is greater than the θ values seen in drop tests. The average θ during normal descent is around 15°, and the maximum θ does not usually exceed 25°. We used $\theta_{\text{INIT}} = 35^\circ$ only to cause a large perturbation in order to analyze the dynamic response of the parachute cluster. All of the θ_{INIT} comparison computations used the PTE configuration.

The parachute described in [11] uses a reefing technique to permit incremental opening of the canopy. The parachute skirt is initially constricted by reefing lines and the reefing lines are cut at predetermined time intervals to allow the canopy to "disreef" to larger diameters. In the third set of computations, two scenarios were computed to analyze how conditions immediately after disreefing could have an effect on long-term dynamics. In the first scenario, which we call "simulated disreef", $\theta_{\text{INIT}} = 10^\circ$, and for both parachutes $D_{\text{INIT}} = 70$ ft. These values represent the approximate θ during final disreefing and the average minimum D during nominal descent. The second scenario represents an "asynchronous disreef" by using for one parachute $D_{\text{INIT}} = 70$ ft, and for the other $D_{\text{INIT}} = 90$ ft. These values represent the average minimum and maximum parachute diameters during nominal descent, respectively. Both scenarios used the PTE configuration.

2.1 Starting conditions

Before an FSI computation is started, a series of pre-FSI computations are carried out to build a good starting condition. For the process of building the starting condition, we refer the reader to [11].

2.2 Computational conditions

Figure 2 shows, for a single parachute, the canopy structure mesh and the fluid mechanics interface mesh. The fluid mechanics mesh is cylindrical with a diameter of 1,740 ft and a height of 1,566 ft. It consists of four-node tetrahedral elements, while the fluid interface mesh consists of three-node triangular elements. The number of nodes and elements are given in Table 1. The porosity model is HMGP-FG. The interface-stress projection is based on the SSP. For more information on the computational conditions, we refer the reader to [11]. We computed each parachute cluster for a total of about 75 s, with remesh as needed to preserve mesh quality. The frequency of remeshing varies for each compu-

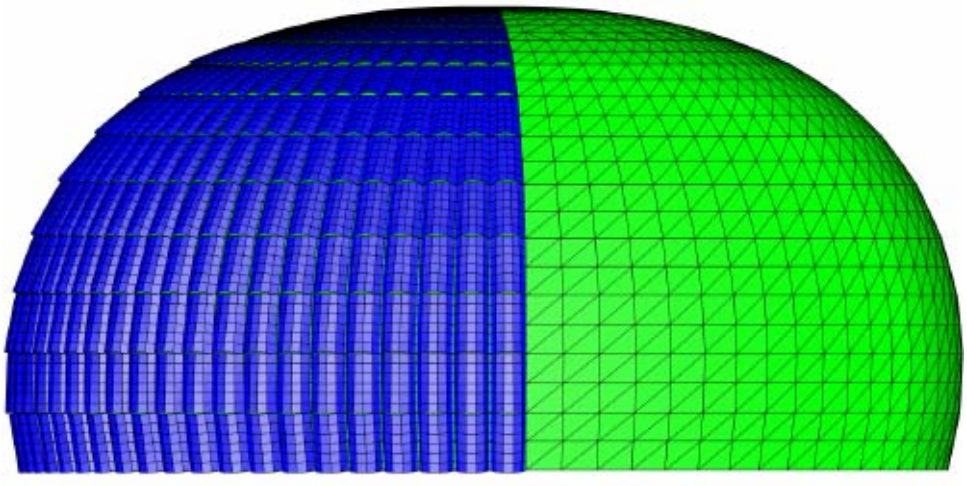

Figure 2: Canopy structure mesh (left) and fluid mechanics interface mesh (right) for a single parachute. The structure has 30,722 nodes, 26,000 four-node quadrilateral membrane elements, and 12,521 two-node cable elements. There are 29,200 nodes on the canopy. The fluid mechanics interface mesh has 2,140 nodes and 4,180 three-node triangular elements.

tation and usually depends on how often the parachutes collide, how much the cluster rotates about the vertical axis, and how much each parachute rotates about its own axis. Depending on the computation, remeshing was needed every 170 to 370 time steps.

2.3 Results

Figures 3–6 show the descent speed U and the drag coefficient, which is calculated as $C_{\rm D} = W/(\frac{1}{2}\rho U^2 S_{\rm o})$, where W is the payload weight, ρ is the density of the air, and $S_{\rm o}$ is the nominal area of the parachute.

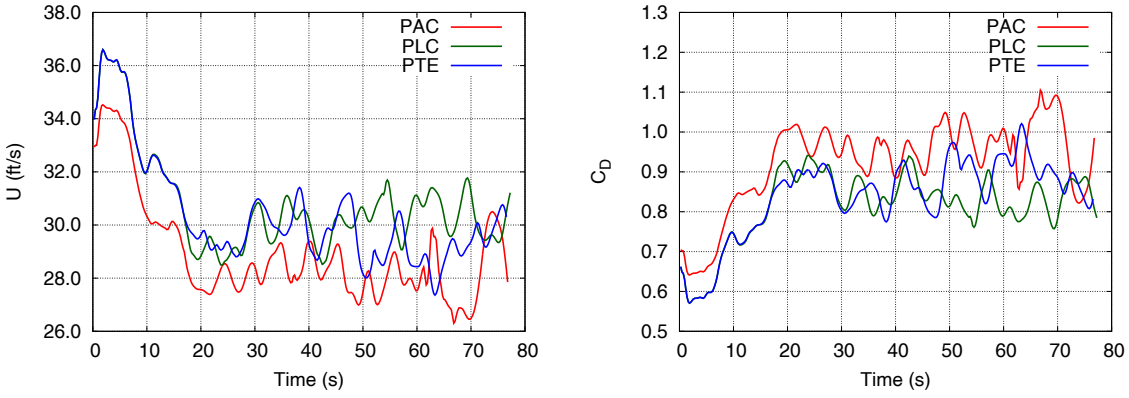

Figure 3: Cluster computations for different payload models and $\theta_{\rm INIT} = 35°$.

Structure		nn	61,443
	Membrane	ne	52,000
	Cable	ne	25,042
	Payload	ne	1
	Interface	nn	58,400
		ne	52,000
Fluid	Interface	nn	4,280
		ne	8,360
	Volume (15°, 80/80 ft)	nn	197,288
		ne	1,210,349
	Volume (25°, 80/80 ft)	nn	280,601
		ne	1,739,739
	Volume (35°, 80/80 ft)	nn	289,679
		ne	1,797,003
	Volume (10°, 70/70 ft)	nn	352,861
		ne	2,199,472
	Volume (35°, 70/90 ft)	nn	289,221
		ne	1,795,542

Table 1: Number of nodes and elements for the two-parachute clusters before any payload modifications. Here nn and ne are number of nodes and elements, respectively. The fluid mechanics volume mesh is tabulated for different combinations of θ_{INIT} and D_{INIT} values. The PLC configuration has 1 more structure node and 1 more cable element. The PTE configuration has 10 more structure nodes, 5 more cable elements, 26 more truss elements, and 8 more payload elements.

Figures 7–8 show the contact between two parachutes from the asynchronous-disreef computation. Figures 9–12 show the vent-separation distance (L_{VS}) for all cluster computations. The horizontal black line on each plot shows the approximate vent-separation distance when the parachutes are in contact. Tables 2–4 summarize the payload descent speeds and drag coefficients for all of the cluster computations.

Payload Model	U (ft/s)	C_{D}
PAC	28.1	0.97
PLC	30.1	0.85
PTE	29.5	0.88

Table 2: Average U and C_{D} for different payload models with $\theta_{\text{INIT}} = 35°$. Statistical analysis begins 20 s after the start of the computation.

3 CONCLUDING REMARKS

We have presented our FSI computations of clusters of large ringsail parachutes, which are constructed from membranes and cables with hundreds of ring gaps and sail slits. The core technology is the SSTFSI technique, supplemented with special FSI techniques. Many

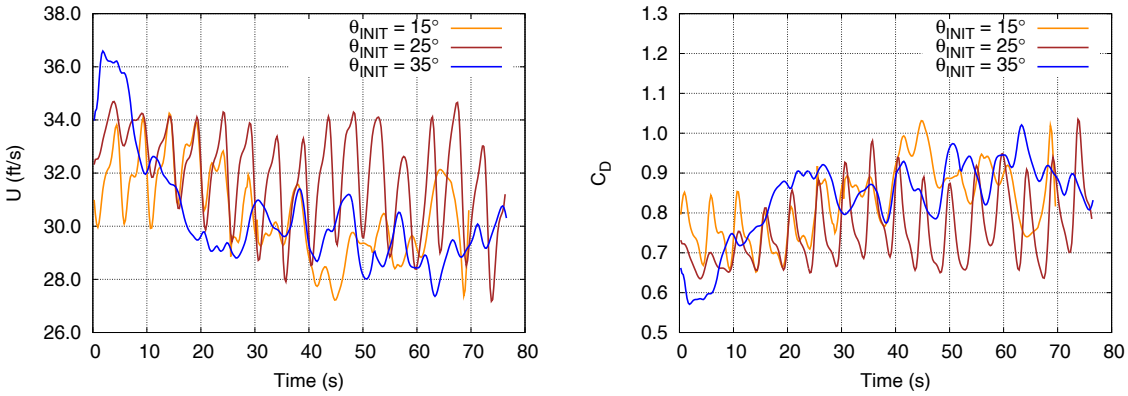

Figure 4: Cluster computations for PTE and different θ_{INIT} values.

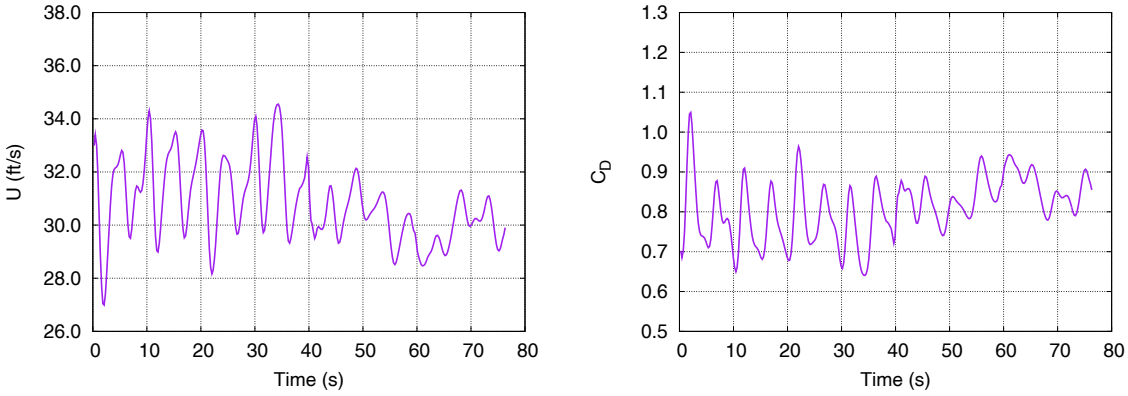

Figure 5: Cluster computations for simulated disreef.

of the special techniques were developed to address the challenges involved in computer modeling of ringsail parachutes. They include the homogenization techniques that make the problem tractable despite hundreds of gaps and slits. Another special technique addresses the computational challenge created by the contact between the parachutes of a cluster. We have also presented a dynamical analysis of the computed results.

ACKNOWLEDGMENT

This work was supported by NASA Grant NNX09AM89G, and also in part by the Rice Computational Research Cluster funded by NSF Grant CNS-0821727.

REFERENCES

[1] T.E. Tezduyar and S. Sathe, "Modeling of fluid–structure interactions with the space–time finite elements: Solution techniques", *International Journal for Numerical Methods in Fluids*, **54** (2007) 855–900, doi: 10.1002/fld.1430.

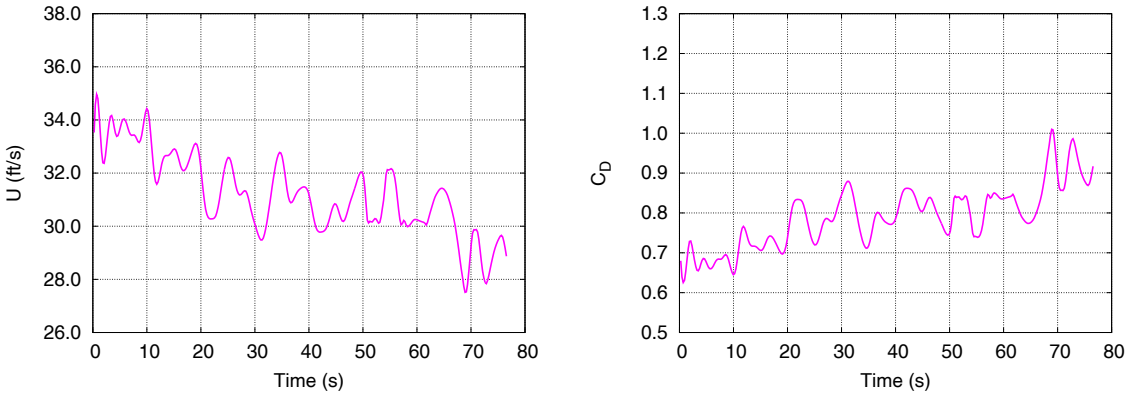

Figure 6: Cluster computations for asynchronous disreef.

θ_{INIT}	U (ft/s)	C_{D}
15°	29.9	0.86
25°	31.4	0.78
35°	29.5	0.88

Table 3: Average U and C_{D} for PTE and different values of θ_{INIT}. Statistical analysis begins 20 s after the start of the computation.

[2] T.E. Tezduyar, "Stabilized finite element formulations for incompressible flow computations", *Advances in Applied Mechanics*, **28** (1992) 1–44, doi: 10.1016/S0065-2156(08)70153-4.

[3] T.E. Tezduyar, M. Behr, and J. Liou, "A new strategy for finite element computations involving moving boundaries and interfaces – the deforming-spatial-domain/space–time procedure: I. The concept and the preliminary numerical tests", *Computer Methods in Applied Mechanics and Engineering*, **94** (1992) 339–351, doi: 10.1016/0045-7825(92)90059-S.

[4] T.E. Tezduyar, M. Behr, S. Mittal, and J. Liou, "A new strategy for finite element computations involving moving boundaries and interfaces – the deforming-spatial-domain/space–time procedure: II. Computation of free-surface flows, two-

	U (ft/s)	C_{D}
Simulated Disreef	30.6	0.82
Asynchronous Disreef	30.8	0.81

Table 4: Average U and C_{D} for the disreef cases. Statistical analysis begins 5 s after the start of the computation for the simulated-disreef case, and 20 s after the start of the computation for the asynchronous-disreef case.

Figure 7: Parachutes at $t = 52.20$ s, $t = 53.36$ s and $t = 54.52$ s during the asynchronous-disreef computation modeling the contact between parachutes.

liquid flows, and flows with drifting cylinders", *Computer Methods in Applied Mechanics and Engineering*, **94** (1992) 353–371, doi: 10.1016/0045-7825(92)90060-W.

[5] T.E. Tezduyar, "Computation of moving boundaries and interfaces and stabilization parameters", *International Journal for Numerical Methods in Fluids*, **43** (2003) 555–575, doi: 10.1002/fld.505.

[6] T.E. Tezduyar, S. Sathe, J. Pausewang, M. Schwaab, J. Christopher, and J. Crabtree, "Interface projection techniques for fluid–structure interaction modeling with moving-mesh methods", *Computational Mechanics*, **43** (2008) 39–49, doi: 10.1007/s00466-008-0261-7.

[7] T.E. Tezduyar, S. Sathe, J. Pausewang, M. Schwaab, J. Christopher, and J. Crabtree, "Fluid–structure interaction modeling of ringsail parachutes", *Computational Mechanics*, **43** (2008) 133–142, doi: 10.1007/s00466-008-0260-8.

[8] T.E. Tezduyar, K. Takizawa, C. Moorman, S. Wright, and J. Christopher, "Space–time finite element computation of complex fluid–structure interactions", *International Journal for Numerical Methods in Fluids*, **64** (2010) 1201–1218, doi: 10.1002/fld.2221.

[9] K. Takizawa, C. Moorman, S. Wright, T. Spielman, and T.E. Tezduyar, "Fluid–structure interaction modeling and performance analysis of the Orion spacecraft

Figure 8: Parachutes at $t = 55.68$ s, $t = 56.84$ s and $t = 58.00$ s during the asynchronous-disreef computation modeling the contact between parachutes.

parachutes", *International Journal for Numerical Methods in Fluids*, **65** (2011) 271–285, doi: 10.1002/fld.2348.

[10] K. Takizawa, S. Wright, C. Moorman, and T.E. Tezduyar, "Fluid–structure interaction modeling of parachute clusters", *International Journal for Numerical Methods in Fluids*, **65** (2011) 286–307, doi: 10.1002/fld.2359.

[11] K. Takizawa, T. Spielman, and T.E. Tezduyar, "Space–time FSI modeling and dynamical analysis of spacecraft parachutes and parachute clusters", *Computational Mechanics*, published online, DOI: 10.1007/s00466-011-0590-9, April 2011, doi: 10.1007/s00466-011-0590-9.

[12] K. Takizawa, T. Spielman, C. Moorman, and T.E. Tezduyar, "Fluid–structure interaction modeling of spacecraft parachutes for simulation-based design", *Journal of Applied Mechanics*, to appear, 2011.

[13] T.E. Tezduyar, S. Sathe, R. Keedy, and K. Stein, "Space–time finite element techniques for computation of fluid–structure interactions", *Computer Methods in Applied Mechanics and Engineering*, **195** (2006) 2002–2027, doi: 10.1016/j.cma.2004.09.014.

[14] K. Takizawa, C. Moorman, S. Wright, J. Christopher, and T.E. Tezduyar, "Wall shear stress calculations in space–time finite element computation of arterial fluid–

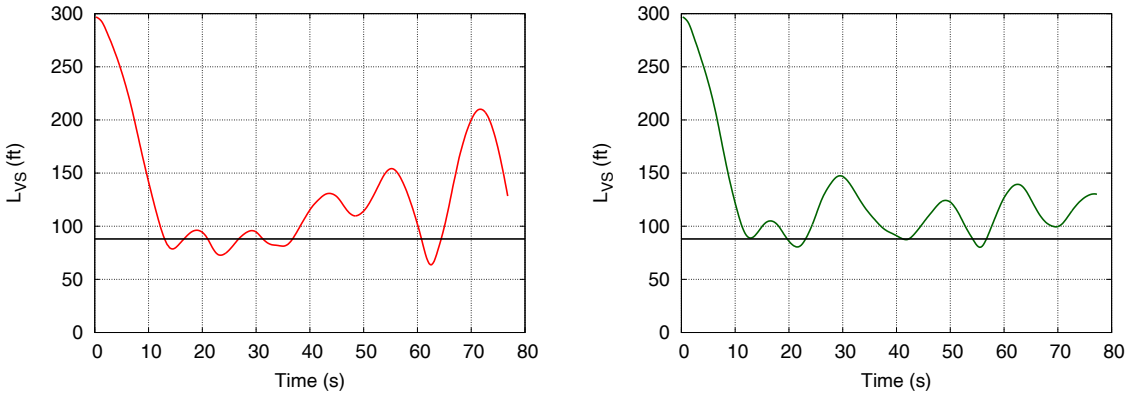

Figure 9: Vent-separation distance. Left: PAC and $\theta_{\mathrm{INIT}} = 35°$, Right: PLC and $\theta_{\mathrm{INIT}} = 35°$.

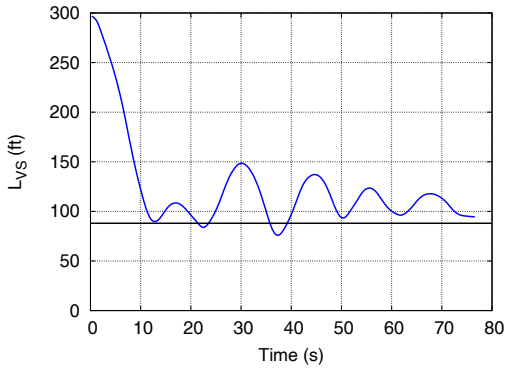

Figure 10: Vent-separation distance. PTE and $\theta_{\mathrm{INIT}} = 35°$.

structure interactions", *Computational Mechanics*, **46** (2010) 31–41, doi: 10.1007/s00466-009-0425-0.

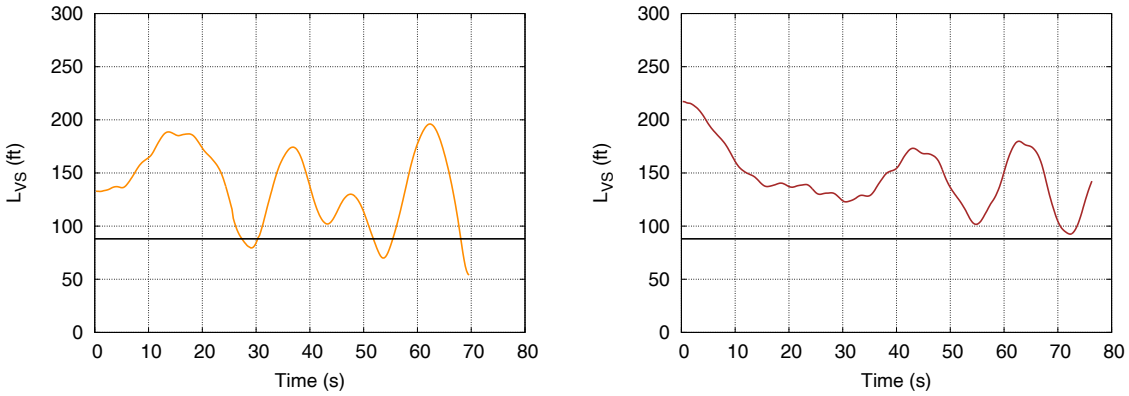

Figure 11: Vent-separation distance. Left: PTE and $\theta_{\mathrm{INIT}} = 15°$, Right: PTE and $\theta_{\mathrm{INIT}} = 25°$.

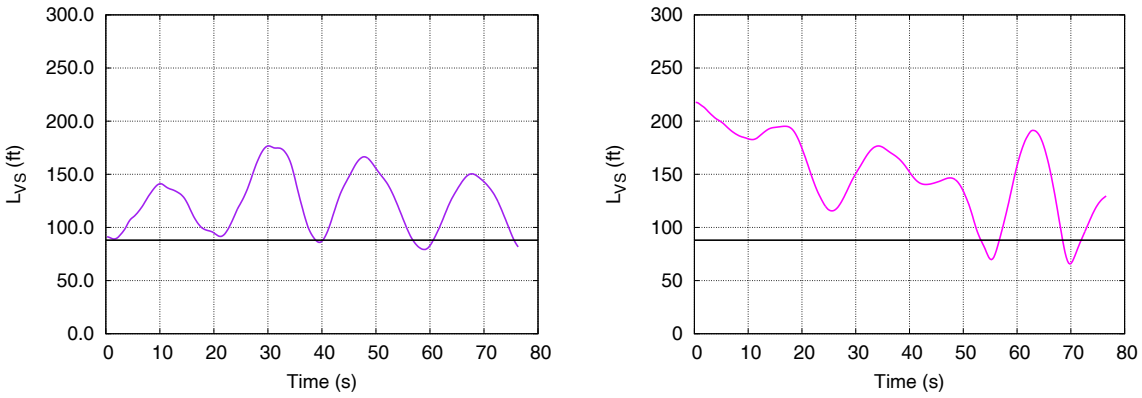

Figure 12: Vent-separation distance. Left: Simulated-disreef, Right: Asynchronous-disreef.